# Electron paramagnetic resonance of ferrite nanoparticles

Yu. A. Koksharov[a)]
*Faculty of Physics, M.V. Lomonosov Moscow State University, 119899 Moscow, Russia*

D. A. Pankratov
*Faculty of Chemistry. M.V. Lomonosov Moscow State University, 119899 Moscow, Russia*

S. P. Gubin
*N.S. Kurnakov Institute of General and Inorganic Chemistry, 117091 Moscow, Russia*

I. D. Kosobudsky
*Saratov State University, Chemical Department, 410026, Saratov, Russia*

M. Beltran and Y. Khodorkovsky
*Beltran, Inc., 1133 East 35th Street, Brooklyn, New York 11210*

A. M. Tishin
*Faculty of Physics, M.V. Lomonosov Moscow State University, 119899 Moscow, Russia*

(Received 23 March 2000; accepted for publication 19 October 2000)

Three types of iron-based oxide nanoparticles (weight compositions $Fe_2O_3$, $BaFe_2O_4$, and $BaFe_{12}O_{19}$) embedded in a polyethylene matrix are studied using the electron paramagnetic resonance technique. All nanoparticles are found to be multiphase. Thermal variations of electron paramagnetic resonance spectra reveal the presence of two phases in the $Fe_2O_3$ nanoparticles. One such phase undergoes an antiferromagnetic-like transition near 6 K. Nanoparticles of $BaFe_2O_4$ demonstrate a resonance anomaly near 125 K that could indicate the presence of a magnetic phase. Reduced magnetic anisotropy in $BaFe_{12}O_{19}$ nanoparticles may be related to either structural imperfection or particle smallness (effective diameter of less than 10 nm). Our data clearly show that low temperature experiments are desirable for the correct identification of nanoparticles by means of the electron paramagnetic resonance technique. © *2001 American Institute of Physics.* [DOI: 10.1063/1.1332417]

## I. INTRODUCTION

Iron-based oxide materials are technologically important materials in which there is an unceasing interest. Whereas $\gamma$-$Fe_2O_3$ is the most popular general-purpose magnetic tape material,[1] $BaFe_{12}O_{19}$ and its substituted derivatives are considered to be the most promising candidates for use in high-density recording media because of their chemical stability and suitable magnetic characteristics.[2,3] Advanced barium ferrite tapes, which utilize particles with a diameter of 40–50 nm, an aspect ratio near 4 and coercivity of about 2000 Oe, offer superior high-density recording performance.[4] Even the pure-phase $BaFe_{12}O_{19}$ is doped with other cations in order to reduce its magnetocrystalline anisotropy.[5] Several methods are often used to prepare ferrite nanoparticles: glass crystallization,[6] ball milling,[7] chemical coprecipitation,[5,8–10] and the citrate precursor technique.[11] It is quite unpleasant that very unlike magnetic properties have been observed in materials that have a similar nanoparticle size but that were produced by different methods.[12] This may be due to structural order–disorder differences.[12] It was also found, with respect to microcrystalline $\gamma$-$Fe_2O_3$ particles (about 100 nm in diameter), that the degree of order in the distribution of vacancies affects their magnetic properties, suggesting that atoms inside a particle can be significantly influenced by canting effects.[13]

It is interesting to compare the properties of iron-based oxide nanoparticles that have various iron/oxygen ratios, all prepared by the same method. Here we report on an electron paramagnetic resonance study of three types of iron-based oxide nanoparticles with weight compositions of $Fe_2O_3$, $BaFe_2O_4$, and $BaFe_{12}O_{19}$. It is well known that bulk $Fe_2O_3$ exists either as ferromagnetic $\gamma$-$Fe_2O_3$ (maghemite) or antiferromagnetic $\alpha$-$Fe_2O_3$ (hematite).[14] Maghemite nanoparticles seem to be a model for the experimental study of nanoparticles[15–22] and for testing the validity of theoretical concepts.[23,24] Bulk hematite is antiferromagnetic below the Morin temperature ($T_M \approx 260$ K) and weakly ferromagnetic above $T_M$.[25] In hematite nanoparticles, the $T_M$ shifts to helium temperatures and no marked anomalies are revealed in the magnetization near 260 K.[25,26] Nonferromagnetic[27] $BaFe_2O_4$ has a rhombic[28] structure and often appears as an impurity phase during the preparation of $BaFe_{12}O_{19}$.[29] To our knowledge, the present work is the first communication about ferrite $BaFe_2O_4$ in nanoscale form. To date, the preparation of nanoparticles of the barium hexaferrite $BaFe_{12}O_{19}$ has been a difficult task. Only recently $BaFe_{12-2x}Ti_xCo_xO_{19}$ particles with a mean diameter of approximately 8 nm have been prepared as ferrofluid.[6]

[a)]Electronic mail: koksharo@epr.phys.msu.su

 

Electron paramagnetic resonance (EPR) is accepted as a very useful technique to study the properties of bulk paramagnetic compounds,[30] including their transitions to the magnetic ordering state.[31] Below the critical temperature, ferromagnetic (FMR) or antiferromagnetic (AFMR) resonances are usually detected.[32] EPR spectra in paramagnetic samples can give information about the resonance-active ion valence and the symmetry of the ligand environment. Angular variation analyses of FMR signals in ferromagnetic single-crystal and textured samples offer the opportunity to deduce the sign and the value of the magnetic anisotropy. Selected nanoparticle systems (including $\gamma$-$Fe_2O_3$,[21,22,33] $Fe_3O_4$,[34,35] $Mn_{0.6}Fe_{0.4}Fe_2O_4$,[35] and Mn–Zn ferrite[36,37]) were investigated by the EPR method. Unfortunately, in the case of nanoparticles the theory of EPR leaves much to be desired since it either remains semiqualitative[38] or requires laborious numerical calculations.[39,40] However, a study of the thermal variation of EPR spectra in nanoparticles can be very informative because of the high sensitivity of the EPR technique to various phase transitions.[31]

## II. EXPERIMENTAL PROCEDURES

Ferrite nanoparticles were produced by the following method. Metal-containing compounds were dissolved in a volatile solvent; and the solution droplets were then passed into a reaction vessel where a chemical reaction took place to convert the reactants to nanoparticles with the composition of the required ferrite. The liquid droplets were deposited into a heated solution/melt of polymer where the precursors decompose. At a sufficiently high supersaturation, a new particle formation occurs by homogeneous nucleation. Nucleation is followed by particle growth and, for sufficiently high particle concentrations, by coagulation and agglomeration. The process of forming ferrite nanoparticles by droplet decomposition can be viewed in the simplest case as the drying of droplets followed by solid and liquid phase chemical reactions in a ''microreactor''–polymer cavity. Since no metal-containing species leave the particles, the constitution and the particle diameter distribution are determined by the composition of the droplet and the size of the polymer cavity. Our small-angle x-ray scattering experiments showed that the produced nanoparticles have a bimodal log-normal size distribution. The typical median particle diameters of the two modes were 2–5 nm and 10–13 nm. The particles were randomly dispersed in a solid polyethylene matrix and were well prevented from agglomerating. Three types of powderlike samples were prepared with 5% wt. of $Fe_2O_3$, $BaFe_{12}O_{19}$, and $BaFe_2O_4$.

The room temperature Mössbauer spectrum of $Fe_2O_3$ nanoparticles can be presented as a superposition of two doublets with the following parameters: $\delta_1 = 0.24$ mm/s; $\epsilon_1 = 0.84$ mm/s; $\delta_2 = 0.52$ mm/s; $\epsilon_2 = 0.87$ mm/s, where $\delta$ is the isomer shift (relative to $\alpha$-Fe) and $\epsilon$ is the quadrupole splitting. The isomer shift for the bulk $\gamma$-$Fe_2O_3$ (A+B site averaged) is equal to 0.34 mm/s.[41] This value does not change significantly in the case of $\gamma$-$Fe_2O_3$ nanoparticles.[42] The value of $\delta_2$ is close to $\alpha$-$Fe_2O_3$ nanoparticles ($\sim$5 nm) prepared by the sol–gel method.[43] The room-temperature Mössbauer spectrum of the $BaFe_2O_4$ nanoparticles is the sum of a sextet ($\delta_3 = 0.38$ mm/s; the hyperfine field $H_{hf3} = 501$ kOe; $\epsilon_3 = -0.21$ mm/s), a doublet ($\delta_4 = 0.36$; $\epsilon_4 = 0.66$ mm/s), and a singlet ($\delta_5 = 0.65$ mm/s). A similar structure is found for the room temperature Mössbauer spectrum of $BaFe_{12}O_{19}$ nanoparticles: a sextet $\delta_6 = 0.37$ mm/s; a hyperfine field $H_{hf6} = 498$ kOe; $\epsilon_6 = -0.22$ mm/s), a doublet ($\delta_7 = 0.34$; $\epsilon_7 = 0.55$ mm/s) and a singlet ($\delta_8 = 0.59$ mm/s). The result of the Mössbauer measurements allows one to conclude that all nanoparticles are multiphase. The presence of the $\gamma$-$Fe_2O_3$ phase (isomer shift of about 0.35 mm/s) (Ref. 41) and $Fe_3O_4$ (isomer shift of about 0.66 mm/s) (Ref. 44) can be assumed.

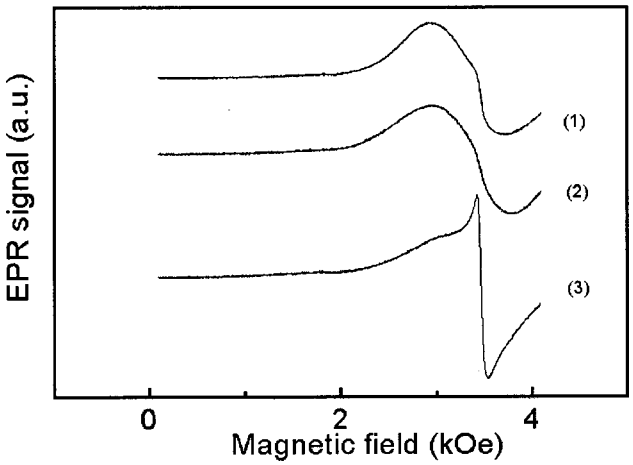


FIG. 1. Room temperature EPR spectra of nanoparticles: $Fe_2O_3$ (curve 1), $BaFe_2O_4$ (curve 2), and $BaFe_{12}O_{19}$ (curve 3).

The EPR experiments were performed with a Varian E-109 spectrometer (*X*-band) with helium flow cryostat (Oxford Instruments) in a temperature range of from 4 K to 170 K. Room temperature EPR spectra were measured using a Varian E-4 spectrometer at 9.18 GHz. The modulation field had a frequency of 100 kHz and an amplitude of 10 Oe. As usual, the EPR signal was the first derivative of the power absorption recorded as a function of the applied magnetic field.

## III. EXPERIMENTAL RESULTS

The experimental EPR spectra of the samples with $Fe_2O_3$, $BaFe_2O_4$, and $BaFe_{12}O_{19}$ nanoparticles embedded in a polyethylene matrix are presented in Figs. 1–3, 5, 8, and 9. At room temperature (RT) the EPR spectra of all the samples show a ''two-line pattern'' (Fig. 1) which is typical of superparamagnetic resonance (SPR) spectra.[40] This spectrum can be considered as a broader line superposed on a narrow line. The relative intensity of these lines depends on the particle size and shape distribution function,[40] as well as on the magnitude of the magnetic anisotropy.[39] For the $Fe_2O_3$ and $BaFe_2O_4$ samples, the broad line predominates in the RT spectra. This line is characterized by a peak-to-peak linewidth of $DH \approx 850$ Oe and an effective *g*-value of approximately 2.07. In the RT spectrum of the $BaFe_{12}O_{19}$ sample, on the contrary, the narrow line is more pronounced, (Fig. 1) with $\Delta H \approx 120$ Oe and $g \approx 2.00$.

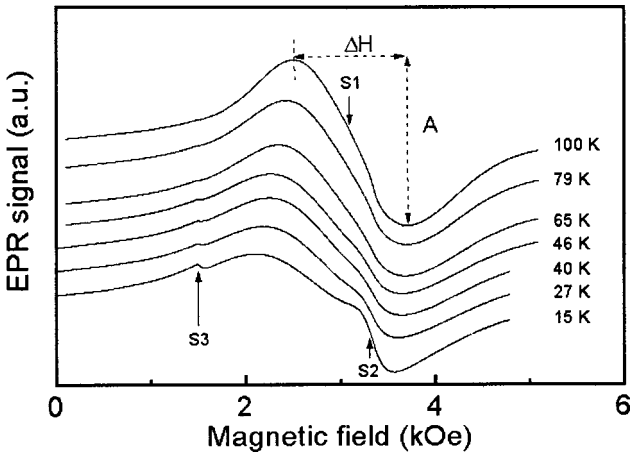


FIG. 2. EPR spectra of $Fe_2O_3$ nanoparticles at different temperature. $\Delta H$ is the peak-to-peak linewidth, $A$ is the EPR signal amplitude. It is presumed that S1 is the superparamagnetic signal ($g=2.12$) from the $\gamma$-$Fe_2O_3$ phase, S2 is the paramagnetic EPR signal ($g=2.02$) from magnetically isolated centers in $\gamma$-$Fe_2O_3$, S3 is the rhombic symmetry signal ($g=4.3$) from the $\alpha$-$Fe_2O_3$ phase.

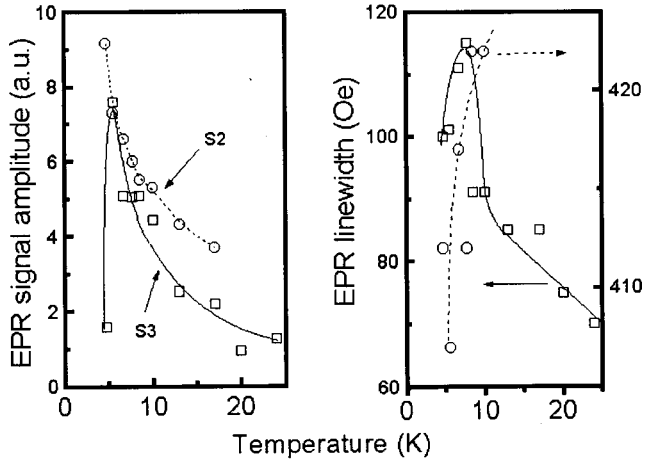


FIG. 4. Thermal variation of the EPR amplitude and linewidth for the signal S2 (circles, dotted lines) and S3 (squares, solid lines). The lines are guides to the eye.

At low temperatures, the EPR spectra of $Fe_2O_3$ change significantly (Fig. 2). On cooling below 100 K down to the lowest reached temperatures, the broad line S1 shows a monotonous increase of the linewidth $\Delta H$ and a decrease of the amplitude $A$ (see the designations in Fig. 2). Such behavior is typical for the SPR of single-domain particles in the absence of transitions to a magnetic ordered state (spin-glass, ''stable state,''[45] etc.). However, below about 50 K new resonances, S2 and S3, appear in the spectra of $Fe_2O_3$ (Figs. 2 and 3). These lines become more noticeable under sample cooling (Fig. 3). Their effective $g$-values are temperature independent and are equal to 2.02 and 4.3 for S2 and S3, correspondingly. The thermal variations of the amplitude and the linewidth of these signals are shown in Fig. 4. It is interesting that S2 behaves like a typical paramagnetic resonance signal, namely, its amplitude grows and the linewidth decreases as the temperature is reduced. On the other hand, the EPR characteristics of S3 demonstrate a phase transition anomaly near 6 K (Fig. 4). The dependencies $\Delta H(T)$ and $A(T)$ have their maximum at $\approx$75 K and $\approx$5.5 K, correspondingly.

EPR spectra of the $BaFe_2O_4$ nanoparticles at different temperatures are shown in Fig. 5. At all temperatures the spectra are broad and rather asymmetric. A significant shift of the line position to low magnetic fields and a marked spectrum broadening are observed at low temperatures (Fig. 5). Anomalies of EPR characteristics take place near 125 K (Fig. 6). Below this temperature the linewidth and the signal amplitude start to change notably (increasing and decreasing, correspondingly).

The thermal variation of EPR spectra of the $BaFe_{12}O_{19}$ sample is typical of SPRs (Fig. 7). The relatively narrow line that dominates at room temperature disappears with the lowering of the temperature (Figs. 8 and 9). Synchronously with the reduction of the narrow signal, a relative growth of the broad resonance takes place, though its absolute amplitude decreases as well. Contrary to the $BaFe_2O_4$, the position of this broad line does not shift so significantly to the lower fields (Fig. 9). Below 10 K a fine structure is visible in the spectra near $g\approx 2$ (Fig. 8).

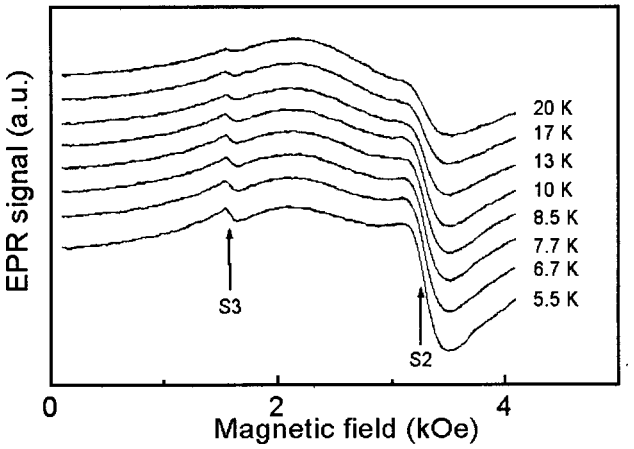


FIG. 3. EPR spectra of $Fe_2O_3$ nanoparticles at low temperatures.

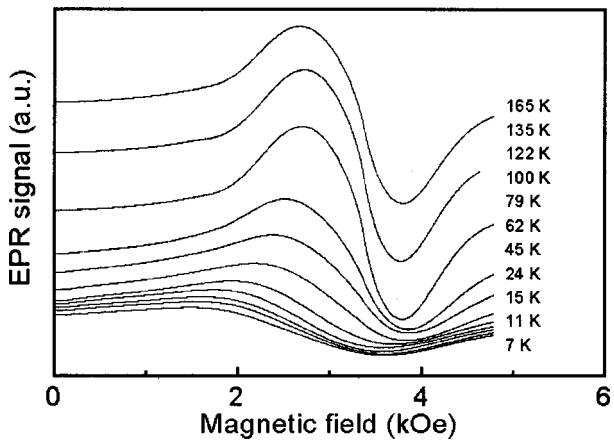


FIG. 5. EPR spectra of the $BaFe_2O_4$ nanoparticles at different temperatures.

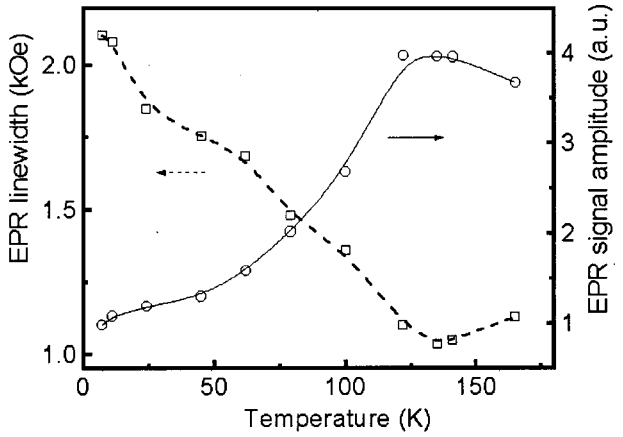


FIG. 6. Thermal variation of the EPR amplitude (circles, solid line) and linewidth (squares, dashed line) for the $BaFe_2O_4$ nanoparticles. The lines are guides for the eye.

## IV. DISCUSSION

It is reasonable to assume that the diversity of EPR properties of the studied nanoparticles results from differences in their interior structures. The bulk counterparts of the investigated oxide nanoparticles also have diverse crystal structures. Maghemite has a spinel structure with a cation distribution $[Fe^{3+}O]\cdot(Fe^{3+})_{5/3}(V)_{1/3}]O_3$, where V is a vacancy.[27] Bulk hematite has a corundum structure.[27] Bulk $BaFe_2O_4$ and $BaFe_{12}O_{19}$ have a rhombic[28] and hexagonal[27] structure, correspondingly. Since the surface/volume ratio is not negligible for nanoparticles, they should be compliant to structural variations that reduce the particle's internal energy. On the other hand, the atomic organizations of a nanoparticle and of its bulk counterpart could correlate to some extent.

It follows that a most complex structure can be expected for $Fe_2O_3$ nanoparticles. Indeed, the bulk thermodynamic Fe–O phase diagram is relatively complicated, with several easily interchangeable iron oxide phases.[46] For objects with reduced dimensionality (nanoparticles, ultrathin films, surfaces, etc.) the mutual phase transformation should be easier.[47] Therefore, one can anticipate a multiphase composition of $Fe_2O_3$ nanoparticles.

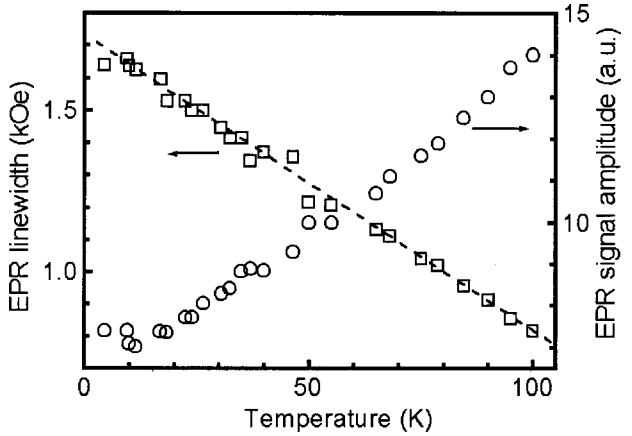


FIG. 7. Thermal variation of the EPR amplitude (circles) and linewidth (squares, dashed line) for the $BaFe_{12}O_{19}$ nanoparticles. The line is a guide for the eye.

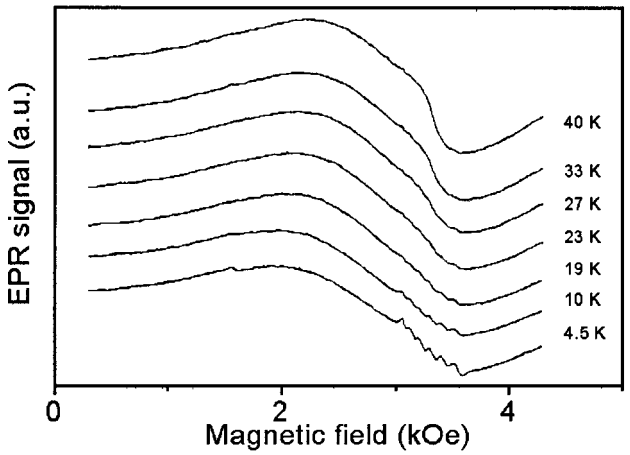


FIG. 8. Low-temperature EPR spectra of $BaFe_{12}O_{19}$ nanoparticles.

First, let us consider the possible origin of the resonances S2 and S3, that appear in the EPR spectra of the $Fe_2O_3$ nanoparticles at low temperatures (Figs. 2 and 3). The value $g=4.3$ for the line S3 is very specific. It is precisely this $g$-value that is characteristic of the high-spin state of $Fe^{3+}$ in the rhombic crystal field.[48,49] A significant departure from axial symmetry can be realized in the rhombohedral $\alpha$-$Fe_2O_3$, as well as in $\gamma$-$Fe_2O_3$ near a defect with an appropriated vacancy distribution. If the latter is the case, the EPR center can be expected to be magnetically isolated and, hence, paramagnetic. The anomaly in $\Delta H(T)$ and $A(T)$ of the S3 signal (Fig. 4) is the evidence of an antiferromagnetic-like transition.[31] This can be a Morin-type transition shifted to the low temperature region.[24,50] Therefore, the S3 signal can be attributed to the $\alpha$-phase of $Fe_2O_3$ particles. This conclusion is also supported by the results of our Mössbauer measurements. On the other hand, the paramagnetic signal S2 ($g=2.02$) may be due to the octahedral symmetry sites of $Fe^{3+}$ in the spinel structure of the $\gamma$-phase. The presence of oxygen vacancies near such centers could break down the exchange interactions that provide the ferrimagnetic properties of the maghemite.

The strongest EPR S1 signal in the $Fe_2O_3$ nanoparticles (Fig. 2) is very similar to the one observed by Gazeau *et al.*

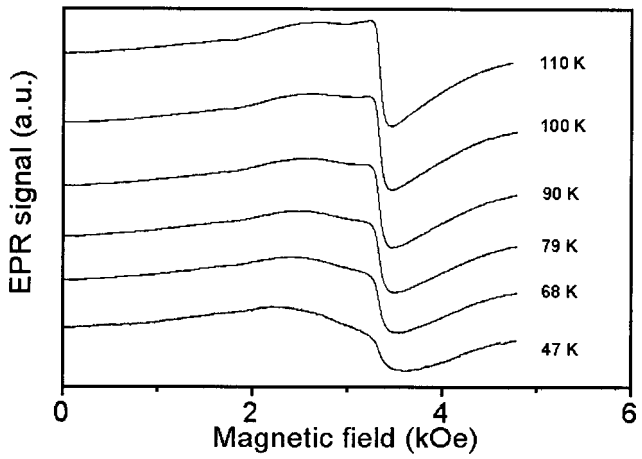


FIG. 9. EPR spectra of $BaFe_{12}O_{19}$ nanoparticles at different temperatures.

in the chemically prepared maghemite nanoparticles of ferrofluids.[21,22] Since S1 is the typical signal of the SPR, we presume that this is due to a ferrimagnetic phase like $\gamma$-$Fe_2O_3$. It should be noted that Gazeau *et al.* probably also detected the S3 signal at low temperatures from the $\alpha$-phase, which, however, was masked by parasite signals.[21]

As already noted, bulk $BaFe_2O_4$ is nonferromagnetic. The strong SPR signal from the $BaFe_2O_4$ nanoparticles (Fig. 5) induces one to think that it is related to a phase with a completely different composition. The EPR anomalies near 125 K (Fig. 6) suggest that such a phase could be the magnetic $Fe_3O_4$. Indeed, bulk magnetite undergoes the Verwey transition at 119 K.[27] Unfortunately, only room temperature data exist on the EPR properties of $Fe_3O_4$ nanoparticles (average diameter about 10 nm).[34] It is interesting to note that the thermal behavior of the EPR linewidth in $BaFe_2O_4$ nanoparticles closely resembles that of the commercially available nanoparticles (nanocat™).[51] However, there is evidence that indicates that the prevalent phase of nanocat is magnetite.[51] The dependency $\Delta H(T)$ for nanocat shows similar features near 120 K and below 50 K, which can also be seen in Fig. 6. The magnetic anomalies in the temperature range 25–50 K have often been observed in various iron oxide nanoparticles.[20,52,53] The acceleration of the EPR linewidth's broadening below 50 K is probably due to spin-glass freezing phenomena.[52]

Bulk hexaferrite $BaFe_{12}O_{19}$ was the subject of a classic FMR work.[54] This compound is characterized by a very high uniaxial anisotropy ($K_u = 3.3\times10^5$ J/m$^3$, where $K_u$ is an anisotropy energy constant).[27] There are very few works related to hexaferrite nanoparticles.[5,6,55,56] The nanoparticles $BaFe_{12-2x}Ti_xCo_xO_{19}$, with a mean diameter of about 8 nm, revealed[6] $K_u = (0.7-2.4)\times10^5$ J/m$^3$. The fact that in nanoparticles the contribution of the particle's surface to the total magnetic anisotropy could be appreciable[57] and could even dominate[22] the high bulk anisotropy does not guarantee a high value of $K_u$ for the nanoparticles. Another reason for a reduction in the magnetic anisotropy could be various inevitable structural defects in the nanoparticles. A decrease of the anisotropy field due to crystalline defects, stresses, and strains was observed in hexaferrites.[58] The EPR spectra in $BaFe_{12}O_{19}$ nanoparticles (Figs. 8 and 9) revealed the significant effect so superparamagnetic fluctuations resulting in a narrowing of the resonance. This could be evidence of reduced magnetic anisotropy.

However, it is possible that the studied nanoparticles are too small. It was found[56] that for $BaFe_{12}O_{19}$ nanoparticles with an effective diameter of less than approximately 12 nm, the specific magnetization and the coercivity decrease drastically. The appearance of an unusually fine structure in the low temperature spectra (Fig. 8) is not yet comprehensible. It may, again, indicate that these $BaFe_{12}O_{19}$ nanoparticles are multiphase.

## V. CONCLUSIONS

Three types of iron-based oxide (ferrite) nanoparticles in a polyethylene matrix were studied by the EPR technique. The EPR spectra suggest that $Fe_2O_3$ nanoparticles contain ferromagnetic (presumably, $\gamma$-$Fe_2O_3$) and antiferromagnetic ($\alpha$-$Fe_2O_3$) phases. The strong SPR signal ($g\approx2.1$) that dominated at high temperatures in typical of $\gamma$-$Fe_2O_3$ nanoparticles. The weak EPR signal of the rhombic symmetry ($g\approx4.3$) that appears at low temperatures may be attributable to an $\alpha$-$Fe_2O_3$ phase that undergoes an antiferromagnetic-like transition near 6 K. The $BaFe_2O_4$ nanoparticles, the bulk counterpart of which is non-ferrimagnetic, demonstrate an EPR anomaly near 125 K that could indicate the presence of a $Fe_2O_4$ phase. The $BaFe_{12}O_{19}$ nanoparticles reveal an EPR signal that is significantly narrowed at high temperatures by superparamagnetic fluctuations. This is evidence of the reduced magnetic anisotropy energy that may be due to structural imperfections or to the particle's smallness (effective diameter $<10$ nm). A comparison of high- and low-temperature EPR spectra in $Fe_2O_3$ and $BaFe_2O_4$ nanoparticles (Figs. 1, 3, and 5) clearly shows that low temperatures experiments are desirable for the correct identification of nanoparticles by means of the EPR technique.

## ACKNOWLEDGMENT

Yu. A.K. acknowledges the partial support of INTAS (Project No. 99-01086).

[1] *Encyclopedia of Chemical Technology*, edited by J. I. Kroschwitz and M. Howe-Grant (Wiley–Interscience, New York, 1995).
[2] X. Y. Sui and M. H. Kryder, Appl. Phys. Lett. **63**, 1582 (1993).
[3] D. E. Speliotis, J. Magn. Magn. Mater. **193**, 29 (1999).
[4] D. E. Speliotis, IEEE. Trans Magn. **31**, 2877 (1995).
[5] H. C. Fang, Z. Yang, C. K. Ong, Y. Li, and C. S. Wang, J. Magn. Magn. Mater. **187**, 129 (1998).
[6] R. Müller, R. Hiergeist, H. Steinmetz, N. Ayoub, M. Fujisaki, and W. Schüppel, J. Magn. Magn. Mater. **201**, 34 (1999).
[7] G. F. Goya and H. R. Rechenberg, J. Magn. Magn. Mater. **196–197**, 191 (1999).
[8] Q. Chen, A. J. Rondinone, B. C. Chakoumakos, and Z. J. Zhang, J. Magn. Magn. Mater. **194**, 1 (1999).
[9] D. Zins, K. Nakatsuka, F. Gendron, and M. Rivoire, J. Magn. Magn. Mater. **201**, 84 (1999).
[10] D. Prodan, C. Chanéac, E. Tronc, J. P. Jolivet, R. Cherkaour, A. Ezzir, M. Noguès, and J. L. Dormann, J. Magn. Magn. Mater. **203**, 63 (1999).
[11] A. Vijayalakshmi and N. S. Gajbhiye, J. Appl. Phys. **83**, 400 (1998).
[12] M. P. Morales, M. Andres-Vergés, S. Veintmillas-Verdaguer, M. I. Montero, and C. J. Serna, J. Magn. Magn. Mater. **203**, 146 (1999).
[13] M. P. Morales, C. J. Serna, F. Bødker, and S. Mørup, J. Phys.: Condens. Matter **9**, 5461 (1997).
[14] J. B. Goodenough, *Magnetism and the Chemical Bond* (Wiley–Interscience, New York, 1963).
[15] F. T. Parker and A. E. Berkowitz, Phys. Rev. B **44**, 7437 (1991).
[16] J. K. Vassiliou, V. Mehrotra, M. W. Russell, E. P. Giannelis, R. D. McMichael, R. D. Shull, and R. F. Ziolo, J. Appl. Phys. **73**, 5109 (1993).
[17] F. T. Parker, M. W. Foster, D. T. Margulies, and A. E. Berkowitz, Phys. Rev. B **47**, 7885 (1993).
[18] J. L. Dormann, F. D'Orazio, F. Lucari, E. Tronc, P. Prené, J. P. Jolivet, D. Fiorani, R. Cherkaour, and M. Noguès, Phys. Rev. B **53**, 14291 (1996).
[19] B. Martinez, X. Obrados, L. Balcells, A. Rouanet, and C. Monty, Phys. Rev. Lett. **80**, 181 (1998).
[20] B. Martinez, A. Roig, E. Molins, T. González-Carreño, and C. J. Serna, J. Appl. Phys. **83**, 3256 (1998).
[21] F. Gazeau, J. C. Bacri, F. Gendron, R. Perzynski, Yu. L. Raikher, V. I. Stepanov, and E. Dubois, J. Magn. Magn. Mater. **186**, 175 (1998).
[22] F. Gazeau, V. Shilov, J. C. Bacri, E. Dubois, F. Gendron, R. Perzynski, Yu. L. Raikher, and V. I. Stepanov, J. Magn. Magn. Mater. **202**, 535 (1999).
[23] M. F. Hansen and S. Morup, J. Magn. Magn. Mater. **184**, 262 (1998).
[24] J. Dormann, D. Fiorani, and E. Tronc, J. Magn. Magn. Mater. **202**, 251 (1999).

[25] A. M. van der Kraan, Phys. Status Solidi A **18**, 215 (1973).
[26] M. Vasquez-Mansilla, R. D. Zysler, C. Arciprete, M. I. Dimitrijewits, C. Saragovi, and J. M. Greneche, J. Magn. Magn. Mater. **204**, 29 (1999).
[27] J. Smit and H. P. J. Wijn, *Ferrites. Physical Properties of Ferromagnetic Oxides in Relation to Their Technical Applications* (Phillip's Technical Library, New York, 1959).
[28] B. E. Levin, Yu. D. Tretyakov, and L. M. Letuk, *Physical and Chemical Principles of Ferrite Formation. Properties and Applications of Ferrites* (Mettalurgiya, Moscow, 1979).
[29] X. Wang, D. Li, L. Lu, X. Wang, L. Zhang, and Y. Lui, Mater. Lett. **28**, 69 (1996).
[30] A. Abragam and B. Bleaney, *Electron Paramagnetic Resonance of Transition Ions* (Clarendon, Oxford, 1970).
[31] F. J. Owen, Phase Transit. **5**, 81 (1985).
[32] *Ferromagnetic Resonance*, edited by S. V. Vonsovskii (Pergamon, Oxford, 1966).
[33] U. Netzelmann, J. Appl. Phys. **68**, 1800 (1990).
[34] V. K. Sharma and F. Waldner, J. Appl. Phys. **48**, 4298 (1977).
[35] I. Hrianca, I. Malaescu, F. Claici, and C. N. Marin, J. Magn. Magn. Mater. **201**, 126 (1999).
[36] K. Nagata and A. Ishishara, J. Magn. Magn. Mater. **104–107**, 1571 (1992).
[37] R. Massart *et al.*, J. Magn. Magn. Mater. **201**, 73 (1999).
[38] R. S. de Biasi and T. C. Devezas, J. Appl. Phys. **49**, 2466 (1977).
[39] Yu. L. Raikher and V. I. Stepanov, Phys. Rev. B **50**, 6250 (1994).
[40] J. Kliava and R. Berger, J. Magn. Magn. Mater. **205**, 328 (1999).
[41] N. N. Greenwood and T. G. Gibb, *Mössbauer Spectroscopy* (Chapman Hall, London, 1971).
[42] L. Zhang, G. C. Papaefthymiou, and J. Y. Ying, J. Appl. Phys. **81**, 6892 (1997).
[43] V. Vasquez-Mansilla, R. D. Zysler, C. Arciprete, M. I. Dimitrijewits, C. Saragovi, and J. M. Greneche, J. Magn. Magn. Mater. **204**, 29 (1999).
[44] F. T. Parker and A. E. Berkowitz, Phys. Rev. B **44**, 7437 (1991).
[45] I. S. Jacobs and C. P. Bean, in *Magnetism*, edited by G. T. Rado and H. Suhl (Academic, New York, 1963), Vol. 3, p. 271.
[46] D. L. Lindsay, *Oxide Minerals, Short Course Notes* (Mineralogical Society of America, Washington, D.C., 1976), Vol. 3, p. L66.
[47] N. G. Condon, M. B. Leibsle, A. R. Lennie, P. W. Murray, D. J. Vaugham, and G. Thornton, Phys. Rev. Lett. **75**, 1961 (1995).
[48] J. S. Griffith, Mol. Phys. **8**, 213 (1965).
[49] I. Ardelean, M. Peteanu, V. Simon, S. Filip, F. Ciorcas, and I. Todor, J. Magn. Magn. Mater. **196–197**, 257 (1999).
[50] N. Amin and S. Arajs, Phys. Rev. B **35**, 4810 (1987).
[51] M. M. Ibrahim, G. Edwards, M. S. Seehra, B. Ganguly, and G. P. Huffman, J. Appl. Phys. **75**, 5873 (1995).
[52] R. H. Kodama, A. E. Berkowitz, E. J. McNiff, Jr., and S. Foner, J. Appl. Phys. **81**, 5552 (1997).
[53] L. Del Bianco, A. Hernando, M. Mutigner, C. Prados, J. C. Sánchez-Lópes, A. Fernández, C. F. Conde, and A. Conde, J. Appl. Phys. **84**, 2189 (1998).
[54] J. Smit and H. G. Beljers, Philips Res. Rep. **10**, 113 (1955).
[55] M. Garsíadel Muro, X. Batlle, and A. Labarta, J. Magn. Magn. Mater. **196–197**, 138 (1999).
[56] N. Rezlescu, L. Rezlescu, M. L. Craus, and E. Rezlescu, J. Magn. Magn. Mater. **196–197**, 463 (1999).
[57] C. Chen, O. Kitakami, and Y. Shimada, J. Appl. Phys. **84**, 2184 (1998).
[58] J. Ding, R. Street, and H. Nishio, J. Magn. Magn. Mater. **164**, 385 (1996).